This article has been accepted for publication in a future issue of this journal, but has not been fully edited. Content may change prior to final publication. Citation information: DOI 10.1109/JIOT.2018.2876415, IEEE Internet of Things Journal

TV White Space Regulated Broadband Power Line Communication for Point-to-Multipoint Downlink IoT Networks: A Standard Perspective

Mohammad Heggo, *Member, IEEE*, Sumei Sun, *Fellow, IEEE*,
Xu Zhu, *Senior Member, IEEE* and Yi Huang, *Senior Member, IEEE*

***Abstract*—Broadband power line communication (BPLC) and television white space (TVWS) are regarded as promising candidates for indoor broadband applications of the Internet of things (IoT). However, they share the access to the very high frequency (VHF) band, which could cause harmful interference and performance degradation to each other. In this paper, a TVWS regulated BPLC system is proposed for point-to-multipoint downlink communication, which integrates the requirement of primary user sensing and the permissible transmission power spectral density (PSD) for TVWS users into the BPLC standard, regarding VHF band access. This integration guarantees minimum interference level between TVWS and BPLC and allows higher transmission PSD for BPLC users in VHF, and hence higher capacity and coverage for BPLC.**

I. Introduction

The revolutionary development in communication technologies and protocols that took place in the last decade assists information exchange with high speed and large bandwidth. This creates a reliable backhaul network that can support Internet of things (IoT) services, which encompass connecting different objects and sensors with different communication technologies into one network [1] [2]. Television white space (TVWS) communication and broadband power line communication (BPLC) are two promising technologies that introduce cost-effective solutions for high speed applications, especially in the indoor environment [3]–[6]. The two technologies have been recently introduced to support machine-to-machine services in IoT network [7]–[9]. However, TVWS and BPLC share the very high frequency (VHF) band, which can introduce potential interference if they are integrated into the same IoT network. This interference can affect the achievable throughput and coverage distance, which drives our need for deeper study into the regulatory standards of both technologies to achieve better cooperation and integration into an IoT network.

Cognitive access of TVWS spectrum was recommended by the Federal Communication Commission (FCC) in May 2004 [10]. In December 2008, FCC issued the second report [11] to regulate TVWS cognitive communication. The report regulates the transmission power limits over the secondary users (SUs) in order to protect the primary users (PUs) from interference. SUs shall acquire sufficient information about PU activity before utilizing the TV channel. Hence, the SU shall be connected to a geolocation database and/or have high sensing capabilities. The geolocation database has a detailed temporal and geographical map for the availability of PU TV channels.

BPLC has drawn researchers' attention in last decade as a promising technology for high speed indoor applications. However, power line cables have not been designed or shielded to carry the communication signals, which causes communication signal power loss due to electromagnetic radiation [12] [13]. This radiation can cause severe interference to surrounding wireless services, which share the same band in particular, TV and radio wireless services in the VHF band [14]–[16]. Consequently, the electromagnetic compatibility (EMC) regulations limit the power spectral density (PSD) of BPLC transmitter to avoid interference with existing wireless services. For example, the standard of the comité European de normalisation électrotechnique (CENELEC) [6] limits the PSD of BPLC signal to -55 dBm/Hz in the high frequency (HF) band between 1.8 MHz and 30 MHz, and -80 dBm/Hz in the VHF band between 30 MHz and 100 MHz. The 25 dB difference in the allowed PSD between the HF and the VHF band yields a significant degradation in BPLC achievable throughput and coverage distance in VHF band compared to HF band. In [17] and [18], the cooperation was proposed between TVWS and BPLC point-to-point systems in VHF band only from both throughput and regulations perspectives, while an overall TVWS BPLC standard framework for both HF and VHF bands was not considered. Also, the coverage and throughput analysis of the downlink point-to-multipoint TVWS BPLC communication were not addressed.

In this paper, to mitigate the interference challenge in realizing an IoT network, we propose a standard framework which integrates the HomeplugAV2 standard [6] [14] for BPLC and the ECMA-392 standard [19] for TVWS into a point-to-multipoint communication system, which is referred to as high throughput white BPLC (HT-WBPLC). This work is different from the previous work in the following aspects:

1) To the best of our knowledge, this is the first work to investigate the integration of BPLC with TVWS in a downlink point-to-multipoint communication system,

M. Heggo, X. Zhu and Y. Huang are with the Department of Electrical Engineering and Electronics, the University of Liverpool, Liverpool L69 3GJ, UK. X. Zhu is also with HIT (Shenzhen), China. E-mails:{m.heggo, xuzhu, huangyi}@liverpool.ac.uk.

S. Sun is with the Institute for Infocomm Research, Agency for Science, Engineering and Research (A*STAR), Singapore. E-mail: sunsm@i2r.a-star.edu.sg. M. Heggo is also with A*STAR, Singapore. This work has been sponsored by A*STAR under the ARAP scheme and the University of Liverpool.

This article has been accepted for publication in a future issue of this journal, but has not been fully edited. Content may change prior to final publication. Citation information: DOI 10.1109/JIOT.2018.2876415, IEEE Internet of Things Journal

which integrates the requirement of primary user sensing and the permissible transmission power spectral density (PSD) for TVWS users into the BPLC standard. Based on standard compatibility and our channel measurement results, the proposed standard framework enables additional frequency band of 100 MHz - 200 MHz to be used by BPLC, guarantees minimum interference level between TVWS and BPLC and allows higher transmission PSD for BPLC users in VHF. Both coverage and throughput analysis are provided for the proposed HT-WBPLC system. The results obtained show the benefit of utilizing the crosstalk between wireless TVWS and BPLC to enhance the overall HT-WBPLC system performance, especially in the frequency beyond 100 MHz. HT-WBPLC achieves higher throughput and coverage compared to MIMO BPLC.

2) The proposed HT-WBPLC standard framework allows three point-to-multipoint operating modes: a) BPLC in HF, b) TVWS in VHF and in PU absence, and c) BPLC in VHF and in PU presence, according to PU status and operating frequency band, leading to a higher degree of freedom in adapting to different standard requirements of BPLC and TVWS. Resource allocation for the proposed HT-WBPLC standard framework is investigated to maximize the system throughput under different requirements of operating modes, while the previous work on resource allocation for orthogonal frequency division multiple access (OFDMA) based cognitive radio networks [20]–[25] cannot be applied directly, as each operating mode has their specific PSD and subchannel frequency spacing.

The rest of the paper is organized as follows. In Section II, we present the proposed HT-WBPLC system model for IoT network. In Section III, channel measurement results for the cross-talk between wireless TVWS channel and BPLC channel are presented. In Section IV, frequency and power allocation problem for different users is investigated and optimal solution is proposed. In Section V, point-to-multipoint system simulation results are presented to evaluate the performance of our proposed HT-WBPLC system and in comparison to TVWS and MIMO BPLC systems. In Section VI, the paper is concluded.

II. HT-WBPLC: Standard Overview and System Model

A. HT-WBPLC Standard for IoT Networks

The first edition of ECMA-392 [19] standard was released in 2009 for TVWS communications, and the second edition was released in 2012. Also, HomplugAV2 standard [14] was issued in 2012 as an extension to the IEEE 1901 standard for BPLC systems. The common band between ECMA-392 and HomeplugAV2 standards is the VHF band. However, BPLC and TVWS transceivers are permitted to access the VHF band at different transmission PSD levels. BPLC transceiver uses -80 dBm/Hz PSD to access VHF band compared to -47.7 dBm/Hz PSD, in case of TVWS transceiver.

The proposed standard amendment for HT-WBPLC allows the integration of TVWS and BPLC into one communication system in IoT network. Hence, it incorporates both ECMA-392 and HomeplugAV2 standards. HT-WBPLC has three modes of operation according to the frequency band and PU activity. In Fig. 1, different operating modes of HT-WBPLC are mapped over four quadrants, where the upper part of the figure represents PU absence case and the right part represents VHF band access and vice versa. The three HT-WBPLC modes can be explained as:

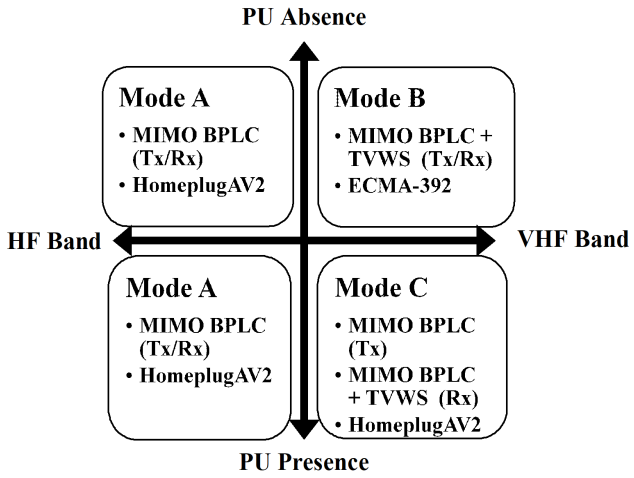

Fig. 1: HT-WBPLC modes of operation

1) Mode A: This mode spans the frequency band 1.8 MHz - 30 MHz. Consequently, HomplugAV2 standard is adopted for the physical (PHY) and medium access control (MAC) layers in communication with transmission signal PSD of -55 dBm/Hz. The band below 30 MHz has the advantage that it is a completely free band, which can provide a backup channel when all TVWS channels are occupied. In WBPLC, single-input single-output (SISO) BPLC is used for communication, while in the HT-WBPLC, MIMO BPLC is used.

2) Mode B: This mode deals with the case of the PU absence in VHF band. Therefore, the spanned frequency spectrum is 54 MHz - 200 MHz. According to FCC regulations, 9 TV channels are allowed for cognitive access in this band which are: 54 MHz - 60 MHz, 60 MHz - 66 MHz, 66 MHz - 72 MHz, 76 MHz - 82 MHz,82 MHz - 88 MHz, 174 MHz - 180 MHz, 180 MHz - 186 MHz, 186 MHz - 192 MHz and 192 MHz - 198 MHz. ECMA-392 standard is adopted in the PHY and MAC layers design. Consequently, the maximum allowed PSD for each 6 MHz channel is -47.7 dBm/Hz and -51.7 dBm/Hz for non-adjacent and adjacent channels, respectively. As a result, our HT-WBPLC system offers BPLC at least 34 dB increase in the PSD in VHF band, hence can significantly improve the achievable throughput. In mode B, BPLC channel is used cooperatively with the wireless TVWS channel, which increases the number of spatial channels.

3) Mode C: This mode deals with the case of the PU presence in VHF band. The spanned frequency band is 30 MHz - 200 MHz. HomeplugAV2 standard is adopted for the PHY and MAC layers of communication. Therefore, the PSD is restricted to -80 dBm/Hz.

The main features of the three modes of HT-WBPLC

This article has been accepted for publication in a future issue of this journal, but has not been fully edited. Content may change prior to final publication. Citation information: DOI 10.1109/JIOT.2018.2876415, IEEE Internet of Things Journal

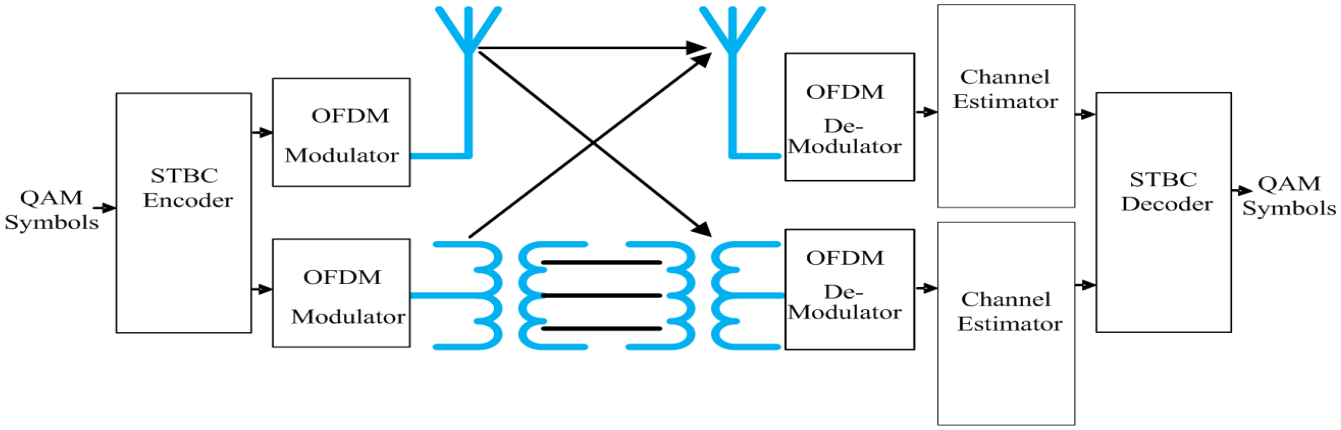

Fig. 2: Block diagram of the HT-WBPLC system

TABLE I: HT-WBPLC Modes of Operation

	Mode A	Mode B	Mode C
Frequency Band	1.8 MHz - 30 MHz	54 MHz - 200 MHz	30 MHz - 200 MHz
Tx Type	BPLC	BPLC + TVWS	BPLC
Rx Type	BPLC	BPLC + TVWS	BPLC + TVWS
Communication Standard	HomeplugAV2	ECMA-392	HomeplugAV2
PSD	-55 dBm/Hz	-47.7 dBm/Hz (free channel), -51.7 dBm/Hz (adjacent channel)	-80 dBm/Hz
Tx/Rx Ports maximum number	2 Tx & 2 Rx	3 Tx & 3 Rx	2 Tx & 3 Rx
Number of Subcarriers	1156	1152	1260
Subcarrier frequency spacing	24.414 kHz	46 kHz	46 kHz

operation are summarized in Table I.

B. HT-WBPLC System Model

In Fig. 2, the system model for HT-WBPLC point-to-multipoint communication system is shown. The model is applied to the three modes of HT-WBPLC operation. The M-ary quadrature amplitude modulation (M-QAM) with gray bit mapping is used as a sub-modulation for the subcarriers in the orthogonal frequency division multiplexing (OFDM) symbol. Each QAM modulated signal is then sent to space time block coding (STBC) encoder, which transmits the same QAM symbol over both BPLC and TVWS channels. The transmission power for each OFDM subcarrier is regulated according to the proposed standard amendment in this section, while the subcarrier and power allocation problem for MIMO HT-WBPLC channel is discussed in detail in Section IV.

III. HT-WBPLC MIMO Channel Model

A. Channel Estimation

HT-WBPLC channel estimation is subdivided into two categories: PU and SU channel estimation. PU channel estimation is obtained using two methods: geolocation database communication and carrier sensing. Each method has its own advantages and drawbacks. Geolocation database communication supports a safer mechanism for the TV band licensed users to protect their network [26] [27]. As a result, the office of communications (Ofcom) in UK stated ”the most important mechanism in the short to medium term will be geolocation” [27]. However, the geolocation database can suffer some prediction errors and differences from real measured PU data as stated in [28], which raises the problems of PU carrier misdetection and false alarm. Hence, sensing techniques are recommended to enhance PU carrier detection. The main challenge of PU carrier sensing is determining the accurate threshold with respect to misdetection and false alarm probabilities [26]. Determining the optimum threshold for PU carrier sensing was approached in our work [17], where the throughput of point-to-point HT-WBPLC system was investigated compared to MIMO BPLC. In [17], a MIMO sensing algorithm was proposed for the PU signal, where probabilities of detection and false alarm of 0.99 and 1e-7 were achieved, respectively.

Regarding SU channel estimation, feedback is assumed between HT-WBPLC Tx and Rx. The impact of channel estimation error on the overall throughput of point-to-point HT-WBPLC system was investigated in our work in [29].

In our paper, we focus on coverage area and throughput analysis of point-to-multipoint HT-WBPLC system compared to MIMO BPLC system in [14], ignoring the channel estimation problems for both PU and SU that had been addressed in previous literature [17] [29]. Perfect channel state information is assumed available for SU Tx and Rx as in [23]–[25] and [30]. We rely on geolocation database communication for PU presence as recommended in [26] and [27].

B. Channel Model

BPLC indoor channel was investigated in VHF band in [31]. The path loss of BPLC was proved to be frequency selective and dependent on several factors like: power line cable type, power outlet density, power line cable branch lengths and terminal loads. Also, VHF path loss model for indoor wireless channel was modelled in [32]. The wireless path loss depends mainly on separating geometric distance, number of

This article has been accepted for publication in a future issue of this journal, but has not been fully edited. Content may change prior to final publication. Citation information: DOI 10.1109/JIOT.2018.2876415, IEEE Internet of Things Journal

separating walls and floors. Moreover, several studies in [33]–[35] suggested enhancing BPLC signal reception by adding an antenna to the receiver and hence, can compromise the radiated electric field.

In this paper, we extend the channel measurements conducted in [13] and [31], to include the crosstalk between BPLC and TVWS wireless channels. The aim of channel measurements is path loss modeling of the crosstalk channel and comparing it against BPLC channel path loss. In [13], BPLC wireless channel measurements in the frequency band 1.7 MHz - 100 MHz show channel capacities of 450 Mbps and 85 Mbps for both short and long distances, respectively. This result proves the promising application of the standard amendment proposed in this paper to regulate HT-WBPLC system. Since, HT-WBPLC is proposed to span VHF band up to 200 MHz, the frequency band of our channel measurements is 84 MHz - 200 MHz. However, we avoid the frequency modulation (FM) band from 88 MHz - 110 MHz due to the interference from FM radio. The channel measurements are held inside the laboratories and offices within the Department of Electrical Engineering and Electronics of the University of Liverpool, which makes the results applicable to indoor office environment. The Tx and Rx are located at the same floor. The channel between any two power line couplers is represented by network of power line cables, while the channel between any two wireless antennas is the radio propagation channel. The path loss is measured using radio frequency (RF) signal generator at Tx and spectrum analyzer at Rx. The path loss is measured for three different channels: 1) the channel between two power line coupling circuits, referred to as h_{11}; 2) the channel between a coupling circuit at Tx and wireless antenna at Rx, referred to as h_{12}; 3) the channel between wireless antenna at Tx and power line coupling circuit at Rx, referred to as h_{21}.

Two broadband coupling circuits have been used in Tx and Rx. The coupling circuit has been designed to be broadband inductive as in [36], to achieve flat gain in broadband application. The loss has been measured in the coupling circuits and the connection cables by measuring their S-parameters using the network analyzer for calibration purpose. The channel measurements have been carried out between the outlets belonging to the same phase and the same distribution box. The channel measurements have been done in different rooms to have an average path loss representation.

In Fig. 3, the gain of the crosstalk and BPLC channels are shown versus distance. The channel gain is measured at four frequencies in the band 84 MHz - 200 MHz, which are 84 MHz, 110 MHz, 140 MHz and 190 MHz. The gain in Fig. 3 is mapped for all aforementioned four frequencies to better describe the path loss in the whole frequency band rather than single frequency tone. The gain is measured for each frequency at different coverage distances to model the path loss of the channel. The channel measurement results show that BPLC and crosstalk channels have close gain performance with respect to distance, since the slope α of the fitted channel gain takes the values of -2.7, -1.8 and -1.4 for the h_{11}, h_{12} and h_{21}, respectively. Also, the results show that the crosstalk channel gain is below BPLC channel gain for small coverage

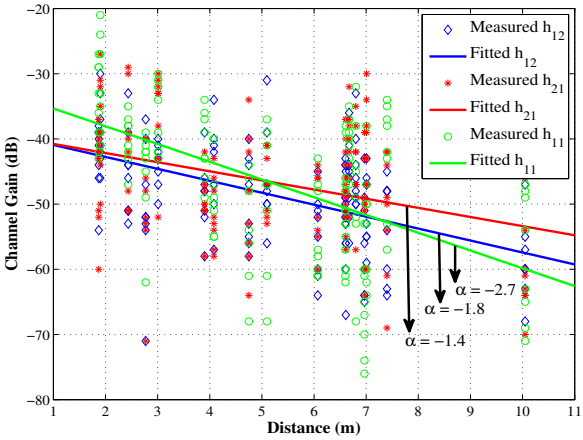

Fig. 3: Crosstalk channel compared to BPLC channel

distance; however for long coverage distances the crosstalk channel gain outperforms the corresponding BPLC channel gain. This is due to the dependence of the crosstalk channel gain mainly on the geometric separation distance between Tx and Rx. However, BPLC channel gain is mainly dependent on the electric separation distance, which is the length of the power line cable connecting the Tx to the Rx. It is known that the electric distance is longer than the geometric distance as reported in [31].

An important observation can be deduced from Fig. 3, which is measured channel gain large variance about its mean value. BPLC channel gain with respect to geometric Tx-Rx distance is characterized by its large variance, as have been proved in previous literature measurements [37]. This is due to BPLC channel gain dependency on Tx-Rx "electric distance" rather than "geometric distance". Also, BPLC channel gain varies according to powerline topology, cable connections, connected loads and outlet density, which increases the overall channel variance about its mean value.

IV. Throughput Maximization and Power Allocation in HT-WBPLC

In this paper, the downlink is investigated for a point-to-multipoint HT-WBPLC indoor system. The sink is connected to a geolocation database to obtain the PU temporal and geographical map of access to the TV channels. Also, the noise is assumed to have zero mean and PSD N_0.

A. Problem Formulation

In HT-WBPLC, there are N_1 subcarriers in HF band 1.8 MHz - 30 MHz. In this band, HT-WBPLC transmitter uses the N_1 subcarriers of BPLC channel only under the PSD constraint of HomeplugAV2 [14]. In VHF band 30 MHz - 200 MHz, there are N_2 subcarriers that are used by HT-WBPLC transmitter under one of the following two conditions:

1) PU absence: In this case, HT-WBPLC transmitter uses both TVWS wireless channel and BPLC channel in the transmission of the data across the N_2 subcarriers. STBC

This article has been accepted for publication in a future issue of this journal, but has not been fully edited. Content may change prior to final publication. Citation information: DOI 10.1109/JIOT.2018.2876415, IEEE Internet of Things Journal

is adopted in the transmission across the two channels in order to enhance the diversity gain. The transmission power is also constrained according to ECMA-392 standard in [19].

2) PU presence: In this case, HT-WBPLC transmitter uses BPLC channel only in the transmission under the PSD constraint of HomeplugAV2. STBC is here adopted in the transmission across MIMO BPLC channels only.

Since we consider the case of downlink between the sink and the users, the target of the power and subcarrier allocation is to achieve maximum throughput and also satisfy different power constraints by different standards at different frequency bands. Let $P_{e_{nj}}$, $2^{k_{nj}}$, P_{nj} be the BER, the constellation size and the allocated power for the n-th subcarrier of the j-th user, respectively, and N_t, N_r, ζ be the numbers of Tx and Rx ports and STBC code rate, respectively. Let $h_{n_t n_r j}$ be the channel gain of spatial path $n_t n_r$ for a given subcarrier and user and $\alpha_{n_t j}$ be the ratio of the power allocated at Tx for each spatial path. Following [38], $\alpha_{n_t j}$ is calculated as

$$\alpha_{n_t j} = \sqrt{\frac{\beta_{n_t j}}{\sum_{n_t=1}^{N_t} \beta_{n_t j}}} \tag{1}$$

where $\beta_{n_t j} = \sum_{n_r=1}^{N_r} |h_{n_t n_r j}|^2$. Let C_{nj} be the effective instantaneous MIMO channel gain for the n-th subcarrier and the j-th user after STBC decoder. C_{nj} can be calculated as $C_{nj} = \sum_{n_t=1}^{N_t} \alpha_{n_t j} \sum_{n_r=1}^{N_r} |h_{n_t n_r j}|^2$. In the case of SISO channel, C_{nj} is simply the channel gain $|h_{n_t n_r j}|^2$ and $\alpha_{n_t j}$ is taken as 1. Hence, a simple approximated probability of error expression can be adopted as in [39]

$$P_{e_{nj}} = \frac{0.2}{\left[1 + \frac{1.6}{2^{k_{nj}}-1} \frac{P_{nj} C_{nj}}{N_t \zeta N_0}\right]^{N_t N_r}} \tag{2}$$

Let the $P_{e_{nj}}$ be the same for all subcarriers and users and equal to the target probability of error P_e. Therefore, the number of bits k_{nj} assigned for subcarrier n and user j is expressed as

$$k_{nj} = \log_2 \frac{1 + 1.6 P_{nj} C_{nj}}{N_t \zeta N_0 \left[(0.2/P_e)^{\frac{1}{N_t N_r}} - 1\right]} \tag{3}$$

The second derivative of k_{nj} with respect to P_{nj} is negative, which proves that Equation (3) is a concave function [40]. k_{nj} has three different expressions according to corresponding HT-WBPLC mode of operation.

1) Mode A: In this mode, BPLC channel is the only channel available and hence, N_{t_A}, N_{r_A} and ζ are assumed to be equal to 1 for WBPLC. However, in HT-WBPLC, N_{t_A} and N_{r_A} are equal to 2. Also, the $P_{n_A j}$ allocated to each subcarrier shall be lower than a maximum power P_A, which is the maximum power that can be allocated to the subcarrier to satisfy PSD constraint of HomeplugAV2 in HF band. The number of bits $k_{n_A j}$ assigned to mode A subcarrier n_A of j-th user can be expressed using (3) as:

$$k_{n_A j} = \log_2 \frac{1 + 1.6 P_{n_A j} C_{n_A j}}{N_{t_A} N_0 \left[(0.2/P_e)^{\frac{1}{N_{t_A} N_{r_A}}} - 1\right]} \tag{4}$$

2) Mode B (30 MHz - 84 MHz & PU absence): In this case both BPLC and TVWS channels are used. Let PH_0 represent the probability of the PU absence. Since the frequency band from 30 MHz to 54 MHz is not allowed for TVWS communication, PH_0 is equal to zero in this band. The number of bits $k^{(0)}_{n_B j}$ assigned to mode B subcarrier n_B of the j-th user can be expressed as

$$k^{(0)}_{n_B j} = PH_0 \log_2 \frac{1 + 1.6 P^{(0)}_{n_B j} C^{(0)}_{n_B j}}{N^{(0)}_{t_B} N_0 \left[(0.2/P_e)^{\frac{1}{N^{(0)}_{t_B} N^{(0)}_{r_B}}} - 1\right]} \tag{5}$$

The allocated power $P^{(0)}_{n_B j}$ for each subcarrier shall be below a maximum power $P^{(0)}_B$ to satisfy Tx power constraint of ECMA-392 standard. $N^{(0)}_{t_B}$ and $N^{(0)}_{r_B}$ take the value of 2 in case of WBPLC and the values of 2 and 3, respectively in case of HT-WBPLC. ζ is taken as 1 for full rate STBC coding, where the superscript (0) indicates the absence of the PU.

3) Mode C (30 MHz - 84 MHz & PU presence): In this case BPLC channel is the only channel used and hence, the $k^{(1)}_{n_B j}$ can be expressed as

$$k^{(1)}_{n_B j} = PH_1 \log_2 \frac{1 + 1.6 P^{(1)}_{n_B j} C^{(1)}_{n_B j}}{N^{(1)}_{t_B} (N_0 + N_p) \left[(0.2/P_e)^{\frac{1}{N^{(1)}_{t_B} N^{(1)}_{r_B}}} - 1\right]} \tag{6}$$

where PH_1 and N_p represent PU presence probability and interference power, respectively. Also, the $P^{(1)}_{n_B j}$ shall be below a certain power $P^{(1)}_B$ to satisfy PSD of HomeplugAV2 in VHF band. Let T be the overall throughput, which can be defined as

$$T = \Pi_{I0}(1 - P_e) \sum_{j=1}^{K} \Big[\sum_{n_1=1}^{N_1} \frac{k_{n_A j}}{t_1} + \frac{\sum_{n_B, n_B=1}^{N_2} (k^{(0)}_{n_B j} + k^{(1)}_{n_B j})}{t_2} \Big] \tag{7}$$

where, Π_{I0} is the steady-state probability of non-burst impulsive state $I0$ of the BPLC channel [41]. T is considered as linear combination of k_{nj}, which is concave function with respect to P_{nj}. As a result, T is considered as concave function with respect to P_{nj}. According to [40], maximizing a concave function is considered a convex optimization problem. Hence, the problem of maximizing overall throughput T can be expressed as

$$\max_{P_{n_A j}, P^{(0)}_{n_B j}, P^{(1)}_{n_B j}} T \tag{8}$$

s.t.

(C1) $P_{n_A j}, P^{(0)}_{n_B j}, P^{(1)}_{n_B j} \geq 0$, (C2) $\sum_{j=1}^{K} P_{n_A j} \leq P_A$,

(C3) $\sum_{j=1}^{K} P^{(0)}_{n_B j} \leq P^{(0)}_B$, (C4) $\sum_{j=1}^{K} P^{(1)}_{n_B j} \leq P^{(1)}_B$,

(C5) $\sum_{j=1}^{K} \big[\sum_{n_A=1}^{N_1} P_{n_A j} + \sum_{n_B=1}^{N_2} PH_0 P^{(0)}_{n_B j} + PH_1 P^{(1)}_{n_B j} \big] \leq P_{in}$,

(C6) $\frac{\sum_{n_A=1}^{N_1} k_{n_A j}}{t_1} + \frac{\sum_{n_B=1}^{N_2} (k^{(0)}_{n_B j} + k^{(1)}_{n_B j})}{t_2} \geq R_j$, where N_1 and N_2 are the number of subcarriers in HF and VHF bands, respectively. Also, t_1 and t_2 are OFDM symbol durations in HomeplugAV2 and ECMA-392 standards, respectively. R_j is the throughput requested for each user. P_{in} is the total input power to the sink.

This article has been accepted for publication in a future issue of this journal, but has not been fully edited. Content may change prior to final publication. Citation information: DOI 10.1109/JIOT.2018.2876415, IEEE Internet of Things Journal

B. Problem Solution

The Lagrangian of the problem can be expressed as

$$\begin{aligned}
L =&\Pi_{I0}(1-P_e)\\
&\sum_{j=1}^{K}\Bigg[\sum_{n_A=1}^{N_1}\frac{1}{t_1}\log_2\{1+\frac{1.6P_{n_Aj}C_{n_Aj}}{N_0\big[(\frac{0.2}{P_e})^{\frac{1}{(N_{t_A}N_{r_A})}}-1\big]}\}+\\
&\sum_{n_B}^{N_2}\frac{PH_0}{t_2}\log_2\{1+\frac{1.6P^{(0)}_{n_Bj}C^{(0)}_{n_Bj}}{(2N_0\big[(\frac{0.2}{P_e})^{\frac{1}{(N^{(0)}_{t_B}N^{(0)}_{r_B})}}-1\big])}\}+\\
&\frac{PH_1}{t_2}\log_2\{1+\frac{1.6P^{(1)}_{n_Bj}C^{(1)}_{n_Bj}}{2(N_0+N_p)\big[(\frac{0.2}{P_e})^{\frac{1}{(N^{(1)}_{t_B}N^{(1)}_{r_B})}}-1\big]}\}\Bigg]-\\
&\lambda\sum_{j=1}^{K}\Bigg[\sum_{n_A=1}^{N_1}P_{n_Aj}+\sum_{n_B=1}^{N_2}PH_0P^{(0)}_{n_Bj}+PH_1P^{(1)}_{n_Bj}\Bigg]+\\
&\lambda P_{in}-\sum_{n_A=1}^{N_1}\mu_{n_A}\Bigg[\sum_{j=1}^{K}P_{n_Aj}-P_A\Bigg]-\\
&\sum_{n_B=1}^{N_2}\mu^{(0)}_{n_B}\Bigg[\sum_{j=1}^{K}P^{(0)}_{n_Bj}-P^{(0)}_B\Bigg]-\\
&\sum_{n_B=1}^{N_2}\mu^{(1)}_{n_B}\Bigg[\sum_{j=1}^{K}P^{(1)}_{n_Bj}-P^{(1)}_B\Bigg]+\\
&\sum_{j=1}^{K}\beta_j\Bigg[\sum_{n_A=1}^{N_1}\frac{1}{t_1}\log_2\{1+\frac{1.6P_{n_Aj}C_{n_Aj}}{N_0\big[(\frac{0.2}{P_e})^{\frac{1}{(N_{t_A}N_{r_A})}}-1\big]}\}+\\
&\sum_{n_B=1}^{N_2}\frac{PH_0}{t_2}\log_2\{1+\frac{1.6P^{(0)}_{n_Bj}C^{(0)}_{n_Bj}}{(2N_0\big[(\frac{0.2}{P_e})^{\frac{1}{(N^{(0)}_{t_B}N^{(0)}_{r_B})}}-1\big])}\}+\\
&\frac{PH_1}{t_2}\log_2\{1+\frac{1.6P^{(1)}_{n_Bj}C^{(1)}_{n_Bj}}{2(N_0+N_p)\big[(\frac{0.2}{P_e})^{\frac{1}{(N^{(1)}_{t_B}N^{(1)}_{r_B})}}-1\big]}\}\Bigg]-\\
&\sum_{j=1}^{K}\beta_jR_j
\end{aligned}\tag{9}$$

where, λ, μ_{n_A}, $\mu^{(0)}_{n_B}$, $\mu^{(1)}_{n_B}$ and β_j are Lagrangian multipliers. Using the primal decomposition method, the problem in (9) can be divided into 3 convex optimization sub-problems. Each sub-problem is further decomposed into single variable convex optimization sub-problems as function of the allocated power to each user and subcarrier as

1) Sub-Problem 1:

$$\begin{aligned}
L_1 =&\Pi_{I0}(1-P_e)\\
&\sum_{j=1}^{K}\sum_{n_A=1}^{N_1}\frac{1+\beta_j}{t_1}\log_2\Bigg\{1+\frac{1.6P_{n_Aj}C_{n_Aj}}{N_0\big[(0.2/P_e)^{\frac{1}{N_{t_A}N_{r_A}}}-1\big]}\Bigg\}-\\
&\sum_{j=1}^{K}\sum_{n_A=1}^{N_1}\lambda P_{n_Aj}-\sum_{n_A=1}^{N_1}\sum_{j=1}^{K}\mu_{n_A}\big[P_{n_Aj}-\frac{P_A}{K}\big]
\end{aligned}\tag{10}$$

The single variable convex sub-problem is represented as

$$\begin{aligned}
f_1(P_{n_Aj}) =&\Pi_{I0}(1-P_e)\\
&\Bigg[\frac{1+\beta_j}{t_1}\log_2\Bigg\{1+\frac{1.6P_{n_Aj}C_{n_Aj}}{N_0\big[(0.2/P_e)^{\frac{1}{N_{t_A}N_{r_A}}}-1\big]}\Bigg\}-\\
&\lambda P_{n_Aj}-\mu_{n_A}\big[P_{n_Aj}-\frac{P_A}{K}\big]\Bigg]
\end{aligned}\tag{11}$$

2) Sub-Problem 2:

$$\begin{aligned}
L_2 =&\Pi_{I0}(1-P_e)\\
&\sum_{j=1}^{K}\sum_{n_B=1}^{N_2}\frac{PH_0(1+\beta_j)}{t_2}\log_2\Bigg\{1+\frac{1.6P^{(0)}_{n_Bj}C^{(0)}_{n_Bj}}{(2N_0\big[(\frac{0.2}{P_e})^{\frac{1}{N^{(0)}_{t_B}N^{(0)}_{r_B}}}-1\big])}\Bigg\}-\\
&\sum_{j=1}^{K}\sum_{n_B=1}^{N_2}\lambda PH_0P^{(0)}_{n_Bj}-\sum_{n_B=1}^{N_2}\sum_{j=1}^{K}\mu^{(0)}_{n_B}\big[P^{(0)}_{n_Bj}-\frac{P^{(0)}_B}{K}\big]
\end{aligned}\tag{12}$$

The single variable convex sub-problem is represented as

$$\begin{aligned}
f_2(P^{(0)}_{n_Bj}) =&\Pi_{I0}(1-P_e)\\
&\Bigg[\frac{PH_0(1+\beta_j)}{t_2}\log_2\Bigg\{1+\frac{1.6P^{(0)}_{n_Bj}C^{(0)}_{n_Bj}}{(2N_0\big[(\frac{0.2}{P_e})^{\frac{1}{N^{(0)}_{t_B}N^{(0)}_{r_B}}}-1\big])}\Bigg\}-\\
&\lambda PH_0P^{(0)}_{n_Bj}-\big[P^{(0)}_{n_Bj}-\frac{P^{(0)}_B}{K}\big]\Bigg]
\end{aligned}\tag{13}$$

3) Sub-Problem 3:

$$\begin{aligned}
L_3 =&\Pi_{I0}(1-P_e)\\
&\sum_{j=1}^{K}\sum_{n_B=1}^{N_2}\frac{PH_1(1+\beta_j)}{t_2}\log_2\Bigg\{1+\frac{1.6P^{(1)}_{n_Bj}C^{(1)}_{n_Bj}}{(2(N_0+N_p)\big[(\frac{0.2}{P_e})^{\frac{1}{(N^{(1)}_{t_B}N^{(1)}_{r_B})}}-1\big])}\Bigg\}\\
&-\sum_{j=1}^{K}\sum_{n_B=1}^{N_2}\lambda PH_1P^{(1)}_{n_Bj}-\sum_{n_B=1}^{N_2}\sum_{j=1}^{K}\mu^{(1)}_{n_B}\big[P^{(1)}_{n_Bj}-\frac{P^{(1)}_B}{K}\big]
\end{aligned}\tag{14}$$

The single variable convex sub-problem is represented as

$$\begin{aligned}
f_3(P^{(1)}_{n_Bj}) =&\Pi_{I0}(1-P_e)\\
&\Bigg[\frac{PH_1(1+\beta_j)}{t_2}\log_2\Bigg\{1+\frac{1.6P^{(1)}_{n_Bj}C^{(1)}_{n_Bj}}{(2(N_0+N_p)\big[(\frac{0.2}{P_e})^{\frac{1}{(N^{(1)}_{t_B}N^{(1)}_{r_B})}}-1\big])}\Bigg\}\\
&-\lambda PH_1P^{(1)}_{n_Bj}-\mu^{(1)}_{n_B}\big[P^{(1)}_{n_Bj}-\frac{P^{(1)}_B}{K}\big]\Bigg]
\end{aligned}\tag{15}$$

After forming the Lagrangian functions and applying the Karush-Kuhn-Tucker (KKT) conditions. The power allocated to each mode of operation for subcarrier n and user j is expressed as

$$\begin{aligned}
P_{n_Aj} =&\\
&\Bigg[\frac{1+\beta_j}{(t_1(\lambda+\mu_{n_A}))}-\frac{N_0\big[(\frac{0.2}{P_e})^{\frac{1}{(N_{t_A}N_{r_A})}}-1\big]}{1.6C_{n_Aj}}\Bigg]
\end{aligned}\tag{16}$$

This article has been accepted for publication in a future issue of this journal, but has not been fully edited. Content may change prior to final publication. Citation information: DOI 10.1109/JIOT.2018.2876415, IEEE Internet of Things Journal

$$P_{n_Bj}^{(0)} = \left[\frac{PH_0(1+\beta_j)}{(t_2(PH_0\lambda+\mu_{n_B}^{(0)}))} - \frac{2N_0\left[(\frac{0.2}{P_e})(\frac{1}{(N_{t_B}^{(0)}N_{r_B}^{(0)})})-1\right]}{1.6C_{n_Bj}^{(0)}}\right] \quad (17)$$

$$P_{n_Bj}^{(1)} = \left[\frac{PH_1(1+\beta_j)}{(t_2(PH_1\lambda+\mu_{n_B}^{(1)}))} - \frac{2(N_0+N_p)\left[(\frac{0.2}{P_e})(\frac{1}{N_{t_B}^{(1)}N_{r_B}^{(1)}})-1\right]}{1.6C_{n_Bj}^{(1)}}\right] \quad (18)$$

Using Equations (16) - (18), the power and subcarriers are allocated for each user according to Algorithm 1

Algorithm 1 Subcarrier and user allocation

Initialization: Set $\phi = \{1 \dots K\}$ as the set of users, $\Omega_T = \{1 \dots N_1\} \cup \{1 \dots N_2\}$ as the set of all available subcarriers for all users. Ω_j is the set of the subcarriers allocated to user $j \in \phi$, $\Omega_j = \{\phi\}$. $\beta_j, \mu_{n_A}, \mu_{n_B}^{(0)}, \mu_{n_B}^{(1)} = 0$.
Allocate the maximum permissible power for each subcarrier $P_{n_Aj} = P_A$, $P_{n_Bj}^{(0)} = P_B^{(0)}, P_{n_Bj}^{(1)} = P_B^{(1)}$.
Start a For loop across the subcarriers of Ω_T
for k=1:N_1 **do**
    Calculate k_{n_Aj}/t_1 or $(k_{n_Bj}^{(0)} + k_{n_Bj}^{(1)})/t_2$ for each user j in ϕ.
    if $k_{n_Aj}/t_1 > k_{n_A(j-1)}/t_1$ **then**
        $j \leftarrow n_A$, $\Omega_T = \Omega_T - n_A$
    else
        if $(k_{n_Bj}^{(0)} + k_{n_Bj}^{(1)})/t_2 > (k_{n_B(j-1)}^{(0)} + k_{n_B(j-1)}^{(1)})/t_2$ **then**
            $j \leftarrow n_B$, $\Omega_T = \Omega_T - n_B$
        end if
    end if
    if R_j is achieved **then**
        $\phi = \phi - j$
    end if
end for
while sum of all transmission power is $\leq P_{in}$ **do**
    Calculate the optimum power using the obtained user-frequency map in the For loop with the aid of equations (16) - (18), and find the appropriate λ using the bisection method.
    if $P_{n_Aj} > \mu_{n_A}$ **then**
        $P_{n_Aj} \leftarrow \mu_{n_A}$
    else
        if $P_{n_Bj}^{(0,1)} > \mu_{n_B}$ **then**
            $P_{n_Bj}^{(0,1)} \leftarrow \mu_{n_B}$
        end if
    end if
end while

V. Numerical Results

In this section, the HT-WBPLC downlink model in Fig. 2 is used for simulation. The PU presence activity is represented using two-state discrete-time Markov chain model (DTMC), where the PU presence steady state probability for each 6 MHz TV channel is taken as 0.2. Also, impulsive noise is represented in our simulations by a two-state DTMC model, where the steady state probability of non impulsive state Π_{I0} is 0.9. The power line topology generator in [42] is used in the simulations to model the power line cable, terminal loads and outlet connection and hence, the power line channel. The topology generator in [42] is used to generate 100 topologies for each case of simulation and to calculate the average throughput. The VHF radio propagation channel is modelled as Rayleigh fading channel with average path loss as in [32]. In the simulations, HT-WBPLC is compared to MIMO BPLC [14] and TVWS systems. TVWS is implemented using ECMA-392 standard [19] and the FCC regulations [11].

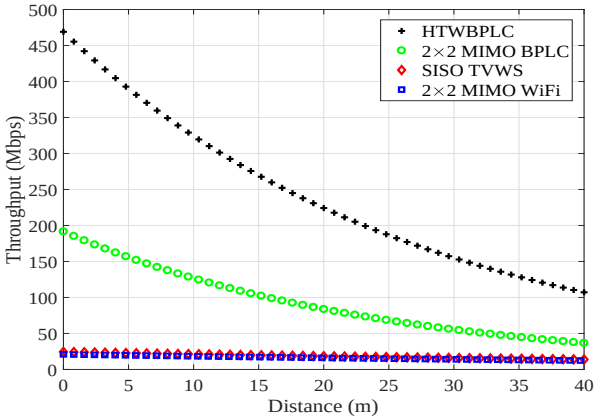

Fig. 4: Achievable throughput versus coverage distance

A. HT-WBPLC Coverage

In Fig. 4, HT-WBPLC coverage distance is compared to those of 2×2 MIMO WiFi, TVWS and MIMO BPLC communication systems, The achievable throughput by the proposed HT-WBPLC nearly doubles that achieved by MIMO BPLC. This proves the ability of our proposed system of improving both the coverage distance and throughput over other communication technologies.

Since the coverage area is considered as a main challenge for current indoor network technologies, a comparison between our proposed HT-WBPLC system and MIMO BPLC system is presented. In the comparison, a $500\ m^2$ area with 20 users is simulated for different BPLC topologies, load connections and users' distribution across the area. The average throughput for each user is calculated and compared against its location with respect to the sink location and hence, a coverage heat map is generated.

In Figs. 5a and 5b the coverage heat maps for HT-WBPLC and MIMO BPLC are presented, respectively. The areas which are covered by throughput ≤ 1 Mbps represent 20% of the total coverage area in MIMO BPLC case, compared to 15% in HT-WBPLC case. This shows the ability of HT-WBPLC to decrease the percentage of areas with limited coverage throughput. For coverage areas $\geq 400\ m^2$ the achieved average throughput per user offered by MIMO BPLC is 17 Mbps, compared to 21.5 Mbps offered by HT-WBPLC for each user.

This article has been accepted for publication in a future issue of this journal, but has not been fully edited. Content may change prior to final publication. Citation information: DOI 10.1109/JIOT.2018.2876415, IEEE Internet of Things Journal

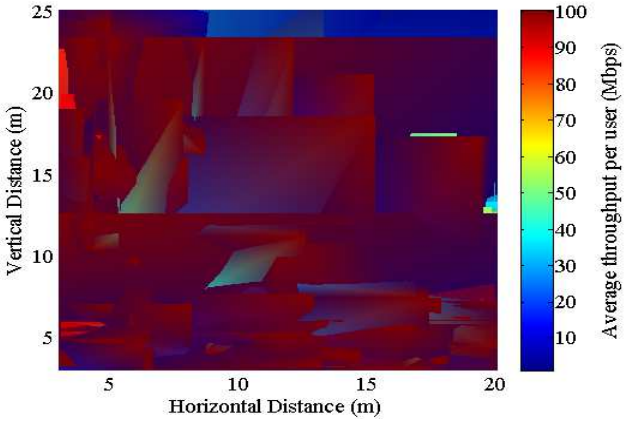

(a)

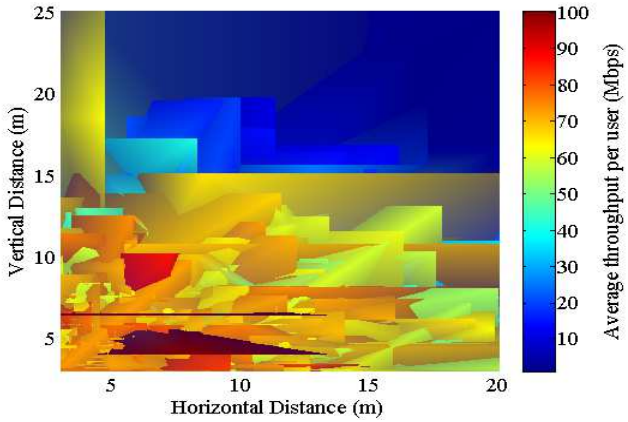

(b)

Fig. 5: Coverage heat map of (a) HT-WBPLC and (b) MIMO BPLC

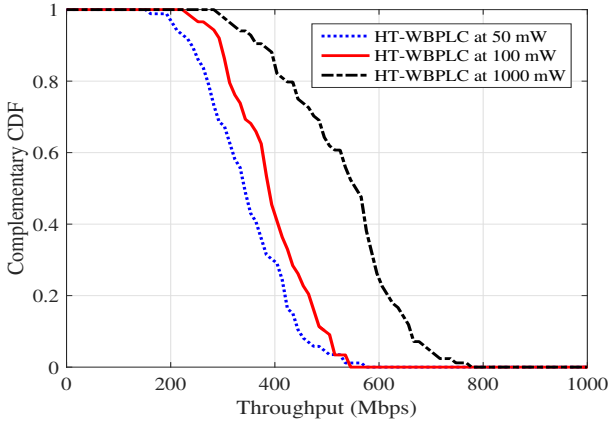

Fig. 6: Complementary CDF of the achievable throughput by the proposed HT-WBPLC using different input power levels

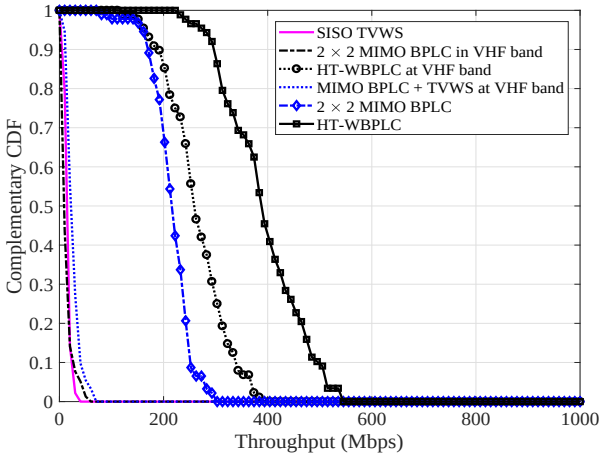

Fig. 7: Complementary CDF of the throughput using the proposed HT-WBPLC and the conventional MIMO BPLC

This shows the ability of HT-WBPLC system to increase the user throughput for large coverage areas by nearly 29% compared to MIMO BPLC.

B. HT-WBPLC Throughput

In Fig. 6, the throughput complementary cumulative distribution function (CCDF) of HT-WBPLC system is shown at different input power levels. The input power levels simulated are 50 mW, 100 mW and 1 W, which are allocated in the downlink for different users and different subcarriers using Algorithm 1 in Section IV. For 50% of the time, HT-WBPLC achieves total downlink throughput of 565 Mbps and 343 Mbps at input transmission power of 50 mW and 1000 mW, respectively. Therefore, an increase of 200 Mbps is observed in the achievable throughput with the increase in the power level. Compared to MIMO BPLC [14], the proposed HT-WBPLC can support higher input power level as it complies with the requirements of the FCC regulations, which allow a 34 dB increase in the PSD than that allowed by HomeplugAV2 for BPLC.

In Fig. 7, our proposed HT-WBPLC is compared to MIMO BPLC in the frequency band 1.8 MHz - 200 MHz at an input transmission power of 100 mW. The simulation results show that for 60% of the time, a throughput of 200 Mbps is achieved using MIMO BPLC [14], while 380 Mbps is achieved using HT-WBPLC which corresponds to 90% increase. Moreover, HT-WBPLC throughput CCDF is compared against MIMO BPLC [14] and TVWS in VHF band only. Significant throughput increase has been shown in VHF band by HT-WBPLC over the other two systems. This proves that the main reason behind the increase in the achievable throughput is due to VHF band exploitation. The increase is for two main reasons: 1) the addition of the wireless channel to the BPLC channel by adding a wireless VHF antenna allows HT-WBPLC to be TVWS standard compliant, which results in higher permissible PSD and hence, higher throughput compared to HomeplugAV2; 2) the increase in allowed spectrum of communication in VHF band up to 200 MHz.

VI. Conclusion

In this paper, a HT-WBPLC communication system has been proposed, which makes use of TVWS and BPLC channels in VHF bands cooperatively, based on the cognitive

radio principle. HT-WBPLC benefits are two-fold: a) HT-WBPLC overcomes IoT network design challenge in realizing an integrated solution that incorporates BPLC and TVWS communication based nodes, by offering a TVWS compliant perspective of BPLC standard, b) HT-WBPLC also overcomes PSD constraints in BPLC and enables transmission in additional frequency band, and hence more coverage area. Our channel measurement results in Section III prove that the crosstalk channel between BPLC and TVWS can be exploited to enhance BPLC signal reception. Point-to-multipoint system simulation results have demonstrated that the proposed HT-WBPLC features a minimum of 40% over MIMO BPLC [14] and TVWS [19] [11], in term of total downlink throughput. Regarding network coverage, HT-WBPLC shows an increase in achievable user throughput by 29% compared to MIMO BPLC [14], for areas larger than or equal to $400\ m^2$. Therefore, HT-WBPLC is a promising solution for the growing needs of IoT.

REFERENCES

[1] A. Al-Fuqaha, M. Guizani, M. Mohammadi, M. Aledhari, and M. Ayyash, "Internet of Things: A Survey on Enabling Technologies, Protocols, and Applications," *IEEE Communications Surveys & Tutorials*, vol. 17, no. 4, pp. 2347–2376, June 2015.

[2] L. Da Xu, W. He, and S. Li, "Internet of Things in Industries: A Survey," *IEEE Transactions on Industrial Informatics*, vol. 10, no. 4, pp. 2233–2243, January 2014.

[3] K.-M. Kang and J. Park, "A New Scheme for Compliance with TV White Space Regulations using Wi-Fi Modules in a Cognitive Radio System," *IEEE Transactions on Consumer Electronics*, vol. 60, no. 4, pp. 567–573, November 2014.

[4] H. Wang, Y. Qian, and H. Sharif, "Multimedia Communications over Cognitive Radio Networks for Smart Grid Applications," *IEEE Wireless Communications*, vol. 20, no. 4, pp. 125–132, August 2013.

[5] M. U. Rehman, S. Wang, Y. Liu, S. Chen, X. Chen, and C. G. Parini, "Achieving High Data Rate in Multiband-OFDM UWB over Power-Line Communication System," *IEEE Transactions on Power Delivery*, vol. 27, no. 3, pp. 1172–1177, July 2012.

[6] H. C. Ferreira, L. Lampe, J. Newbury, T. Swart, and Editors, *Power Line Communications: Theory and Applications for Narrowband and Broadband Communications over Power Lines*. John Wiley & Sons, Inc., 2010.

[7] A. Aijaz and A. H. Aghvami, "Cognitive Machine-to-Machine Communications for Internet-of-Things: A Protocol Stack Perspective," *IEEE Internet of Things Journal*, vol. 2, no. 2, pp. 103–112, April 2015.

[8] H.-C. Hsieh and C.-H. Lai, "Internet of Things Architecture Based on Integrated PLC and 3G Communication Networks," in *IEEE 17th International Conference on Parallel and Distributed Systems (ICPADS)*, pp. 853–856, December 2011, Tainan, Taiwan.

[9] C. Cano, A. Pittolo, D. Malone, L. Lampe, A. M. Tonello, and A. G. Dabak, "State of the Art in Power Line Communications: From the Applications to the Medium," *IEEE Journal on Selected Areas in Communications*, vol. 34, no. 7, pp. 1935–1952, July 2016.

[10] "Notice of Proposed Rule making," *Federal Communications Commision, Document 04–113*, May 2004.

[11] "Second Report and Order and Memorandum Opinion and Order In the Matter of Unlicensed Operation in the TV Broadcast Bands, Additional Spectrum for Unlicensed Devices Below 900 MHz and in the 3 GHz Band," *Federal Communications Commision, Document 08-260*, November 2008.

[12] M. Gebhardt, F. Weinmann, and K. Dostert, "Physical and Regulatory Constraints for Communication over the Power Supply Grid," *IEEE Communications Magazine*, vol. 41, no. 5, pp. 84–90, May 2003.

[13] T. Oliveira, F. Andrade, A. Picorone, H. Latchman, S. Netto, and M. Ribeiro, "Characterization of Hybrid Communication Channel in Indoor Scenario," *Journal of Communication and Information Systems*, vol. 31, no. 1, September 2016.

[14] L. T. Berger, A. Schwager, P. Pagani, and D. Schneider, *MIMO Power Line Communications: Narrow and Broadband Standards, EMC, and Advanced Processing*. CRC Press, 2014.

[15] P. Pagani, R. Razafferson, A. Zeddam, B. Praho, M. Tlich, J.-Y. Baudais, A. Maiga, O. Isson, G. Mijic, K. Kriznar *et al.*, "Electromagnetic Compatibility for Power Line Communications," in *Proc. IEEE 21st International Symposium on Personal Indoor and Mobile Radio Communications (PIMRC)*, pp. 2799–2804, September 2010, Istanbul, Turkey.

[16] T. Ronkainen, R. Vuohtoniemi, and J.-P. Mäkelä, "Radiated Interference of High Frequency Broadband Power Line Communications," in *International Symposium on Electromagnetic Compatibility (EMC Europe)*, pp. 555–559, September 2014,Gothenburg, Sweden.

[17] M. Heggo, X. Zhu, Y. Huang, and S. Sun, "A Hybrid Power Line and TV White Space MIMO System for Indoor Broadband Communications," in *Proc. IEEE 84th Vehicular Technology Conference (VTC) Fall*, September 2016, Montreal, Canada.

[18] M. Heggo, X. Zhu, S. Sumei, and Y. Huang, "White Broadband Power Line Communication: Exploiting the TVWS for Indoor Multimedia Smart Grid Applications," *International Journal of Communication Systems*, vol. 30, no. 16, pp. 1–9, May 2017.

[19] "MAC and PHY for Operation in TV White Space," *ECMA-392*, December 2009.

[20] Y. Zhang and C. Leung, "Resource Allocation in an OFDM-based Cognitive Radio System," *IEEE Transactions on Communications*, vol. 57, no. 7, July 2009.

[21] H. Saki and M. Shikh-Bahaei, "Cross-Layer Resource Allocation for Video Streaming over OFDMA Cognitive Radio Networks," *IEEE Transactions on Multimedia*, vol. 17, no. 3, pp. 333–345, March 2015.

[22] G. I. Tsiropoulos, O. A. Dobre, M. H. Ahmed, and K. E. Baddour, "Radio Resource Allocation Techniques for Efficient Spectrum Access in Cognitive Radio Networks," *IEEE Communications Surveys & Tutorials*, vol. 18, no. 1, pp. 824–847, January 2016.

[23] D. T. Ngo, C. Tellambura, and H. H. Nguyen, "Resource Allocation for OFDMA-based Cognitive Radio Multicast Networks with Primary User Activity Consideration," *IEEE Transactions on Vehicular Technology*, vol. 59, no. 4, pp. 1668–1679, May 2010.

[24] S. Zhang, W. Xu, S. Li, and J. Lin, "Resource Allocation for Multiple Description Coding Multicast in OFDM-based Cognitive Radio Systems with Non-Full Buffer Traffic," in *Proc. IEEE Wireless Communications and Networking Conference (WCNC)*, pp. 199–204, April 2013, Shanghai, China.

[25] K. Yang, W. Xu, S. Li, and J. Lin, "Distributed Multicast Resource Allocation in OFDM-based Cognitive Radio Networks," in *8th International ICST Conference on Communications and Networking in China (CHINACOM)*, pp. 57–62, August 2013, Guilin, China.

[26] D. Makris, G. Gardikis, and A. Kourtis, "Quantifying TV White Space Capacity: A Geolocation-Based Approach," *IEEE Communications Magazine*, vol. 50, no. 9, p. 145, September 2012.

[27] D. Gurney, G. Buchwald, L. Ecklund, S. L. Kuffner, and J. Grosspietsch, "Geo-location Database Ttechniques for Incumbent Protection in the TV White Space," in *Proc. 3rd IEEE Symposium on New Frontiers in Dynamic Spectrum Access Networks*, pp. 1–9, October 2008, Chicago, IL, USA.

[28] A. Achtzehn, J. Riihijarvi, and P. Mahonen, "Improving Aaccuracy for TVWS Geolocation Databases: Results from Measurement-Driven Estimation Approaches," in *Proc. IEEE International Symposium on Dynamic Spectrum Access Networks (DYSPAN)*, pp. 392–403, April 2014, McLean, VA, USA.

[29] M. Heggo, X. Zhu, S. Sun, and Y. Huang, "A Cognitive TV White Space-Broadband Ppower line MIMO Ssystem for Indoor Communication Nnetworks," *Journal of the Franklin Institute*, vol. 355, no. 11, pp. 4755–4770, July 2018.

[30] N. Bounouader, G. Aniba, Z. Guennoun *et al.*, "Exploiting Zero Forcing Bbeamforming and TV White Space Band for Multiuser MIMO Cognitive Cooperative Radio Networks," in *Proc. International Conference on Wireless Networks and Mobile Communications (WINCOM)*, pp. 1–6, October 2015, Marrakech, Morocco.

[31] M. Heggo, X. Zhu, Y. Huang, and S. Sun, "A Novel Statistical Approach of Path Loss Mapping for Indoor Broadband Power Line Communications," in *Proc. IEEE International Conference on Smart Grid Communications (SmartGridComm)*, pp. 499–504, November 2014, Venice, Italy.

[32] J. Andrusenko, R. L. Miller, J. A. Abrahamson, N. M. Merheb Emanuelli, R. S. Pattay, and R. M. Shuford, "VHF General Urban Path Loss Model for Short Range Ground-to-Ground Communications," *IEEE Transactions on Antennas and Propagation*, vol. 56, no. 10, pp. 3302–3310, October 2008.

[33] W. A. Finamore, M. V. Ribeiro, and L. Lampe, "Advancing Power Line Communication: Cognitive, Cooperative, and MIMO Communication,"

in *Proc. Brazilian Telecommunications Symposium*, pp. 13–16, September 2012, Brasilia, Brazil.

[34] P. Degauque, P. Laly, V. Degardin, M. Lienard, and L. Diquelou, "Compromising Electromagnetic Field Radiated by In-House PLC Lines," in *Proc. IEEE Global Telecommunications Conference (GLOBECOM)*, pp. 1–5, December 2010, Miami, Florida, USA.

[35] V. Degardin, P. Laly, M. Lienard, and P. Degauque, "Compromising Radiated Emission from a Power Line Communication Cable," *Journal of Communications Software & Systems*, vol. 7, no. 1, pp. 16–21, March 2011.

[36] S. Chen, *Ultra Wideband Gigabit Powerline Communication*, Ph.D. Dissertation, 2009.

[37] A. M. Tonello and F. Versolatto, "Bottom-up Statistical PLC Channel Modeling-Part II: Inferring the Statistics," *IEEE transactions on Power Delivery*, vol. 25, no. 4, pp. 2356–2363, October 2010.

[38] L. Xian and H. Liu, "An Adaptive Power Allocation Scheme for Space-Time Block Coded MIMO Systems," in *Proc. IEEE Wireless Communications and Networking Conference*, pp. 504–508, March 2005, New Orleans, LA, USA.

[39] D. Wang, H. Minn, and N. Al-Dhahir, "A Robust Asynchronous Multiuser STBC-OFDM Transmission Scheme for Frequency-Selective Channels," *IEEE Transactions on Wireless Communications*, vol. 7, no. 10, pp. 3725–3731, 2008.

[40] S. Boyd and L. Vandenberghe, *Convex Optimization*. Cambridge university press, 2004.

[41] J. Yin, X. Zhu, and Y. Huang, "Modeling of amplitude-correlated and occurrence-dependent impulsive noise for power line communication," in *Proc. IEEE International Conference on Communications (ICC)*, pp. 4565–4570, June 2014, Sydney, Australia.

[42] A. M. Tonello and F. Versolatto, "Bottom-up Statistical PLC channel Modeling-Part I: Random Topology Model and Efficient Transfer Function Computation," *IEEE Transactions on Power Delivery*, vol. 26, no. 2, pp. 891–898, April 2011.

Mohammad Heggo (S'08 - M'17) received his B.Sc. and M.Sc. degrees in Electrical Engineering from Ain Shams University, Cairo, Egypt in 2006 and 2010, respectively. In 2007, he joined the Research and Development department, Elsewedy Electrometer Company, Egypt as an *embedded communication software engineer*. In 2013, he was awarded a dual Ph.D. scholarship for four years from the Electrical Engineering and Electronics at the University of Liverpool, UK and the Cognitive Communications Technology Department, Agency for Science, Technology, and Research, Singapore. He was awarded his Ph.D. degree in electrical engineering from the University of Liverpool, UK in 2017. Currently, he is a *research associate* at the Electrical Engineering and Electronics department, University of Manchester, UK. His research interests include power line communication, electromagnetic interference to transmission lines, cognitive radio, MIMO communication systems and smart grid communications.

Sumei Sun (F'16) is currently *Head* of the Communications and Networks Cluster, and *Lead Principal Investigator* of the Industrial Internet of Things Research Program at the Institute for Infocomm Research, Agency for Science, Technology, and Research, Singapore. Her current research interests are in cognitive communications and networks, next-generation machine-type communications, and industrial internet of things. She is a *Distinguished Speaker* of the IEEE Vehicular Technology Society 2018-2021, *Vice Director* of IEEE Communications Society Asia Pacific Board, and *Chapter Coordinator* of Asia Pacific Region in the IEEE Vehicular Technologies Society. She is also serving as a *member* of the IEEE Communications Society Globecom/ICC Management and Strategy (GIMS) Standing Committee, *an Area Editor* of IEEE Transactions on Vehicular Technology, *Editor* of the IEEE Communications Surveys and Tutorials, and *member* of the IEEE Transactions on Wireless Communications Steering Committee.

Xu Zhu (S'02-M'03-SM'12) received the B.Eng. degree (with the first-class Hons.) in electronics and information engineering from Huazhong University of Science and Technology, Wuhan, China, in 1999, and the Ph.D. degree in electrical and electronic engineering from The Hong Kong University of Science and Technology, Hong Kong, in 2003. She joined the Department of Electrical Engineering and Electronics, University of Liverpool, Liverpool, U.K. in 2003, where she is currently a *Reader*. She is also with the Harbin Institute of Technology, Shenzhen, China. She has more than 160 peer-reviewed publications on communications and signal processing. Her research interests include MIMO, channel equalization, resource allocation, cooperative communications, green communications, etc. She was an *Editor* for the IEEE TRANSACTIONS ON WIRELESS COMMUNICATIONS from 2012 to 2017, and a *Guest Editor* for a number of international journals such as Electronics. She has served as a *chair* for various international conferences, such as Symposium *Co-Chair* of IEEE ICC 2016 and 2019, *Vice-Chair* of the 2006 and 2008 ICARN International Workshops, *Program Chair* of ICSAI 2012, and *Publicity Chair* of IEEE IUCC-2016.

Yi Huang (S'91 - M'96 - SM'06) received BSc in Physics (Wuhan University, China) in 1984, MSc (Eng) in Microwave Engineering (NRIET, Nanjing, China) in 1987, and DPhil in Communications from the University of Oxford, UK in 1994. He has been conducting research in the areas of wireless communications, applied electromagnetics, radar and antennas since 1987. His experience includes 3 years spent with NRIET (China) as a Radar Engineer and various periods with the Universities of Birmingham, Oxford, and Essex at the UK as a member of research staff. He worked as a Research Fellow at British Telecom Labs in 1994, and then joined the Department of Electrical Engineering & Electronics, the University of Liverpool, UK as a Faculty in 1995, where he is now a full *Professor in Wireless Engineering, the Head of High Frequency Engineering Group and Deputy Head of Department*. Prof. Huang has published over 350 refereed papers in leading international journals and conference proceedings, and authored *Antennas: from Theory to Practice* (John Wiley, 2008) and *Reverberation Chambers: Theory and Applications to EMC and Antenna Measurements* (John Wiley, 2016). He has received many research grants from research councils, government agencies, charity, EU and industry, acted as a consultant to various companies, and served on a number of national and international technical committees and been an *Editor, Associate Editor or Guest Editor* of five international journals. He has been a keynote/invited speaker and organiser of many conferences and workshops (e.g. WiCom 2006, 2010, IEEE iWAT2010, LAPC2012 and EuCAP2018). He is at present the *Editor-in-Chief* of Wireless Engineering and Technology, *Associate Editor* of IEEE Antennas and Wireless Propagation Letters, *UK and Ireland Rep* to European Association of Antenna and Propagation (EurAAP), a *Senior Member* of IEEE, a *Fellow* of IET, and *Senior Fellow* of HEA.